

FIRE PROPAGATION IN CYLINDRICAL LI-ION BATTERIES UNDER ULTRA-HIGH STRAIN-RATE DEFORMATION

**Jinyong Kim,¹ PhD Anudeep Mallarapu,¹ Shriram Santhanagopalan,¹ PhD
Yi Ding,² PhD**

¹Energy Conversion and Storage Systems, National Renewable Energy Laboratory,
Golden CO

²Ground Vehicle Systems Center, Warren MI

ABSTRACT

Abuse response of lithium-ion batteries has been extensively studied over several decades. Most studies on the onset and propagation of battery fires following mechanical deformation are focused on understanding the onset of thermal events following quasi-static loading. Using an array of cylindrical lithium-ion cells as example, we report results from ultra-high strain-rate deformation mechanical events (> 100 /s) that result in electrochemical short-circuits followed by thermal events. We present a methodology that takes stock of gas compositions as a function of state of charge and compute flammability limits. Finally, we discuss implications for flame lengths and propensity for propagation of thermal events.

Citation: J. Kim, A. Mallarapu, S. Santhanagopalan, Y. Ding, "Propagation of Fire in Li-Ion Batteries under Ultra-High Strain-Rate Deformation" In *Proceedings of the Ground Vehicle Systems Engineering and Technology Symposium* (GVSETS), NDIA, Novi, MI, Aug. 16-18, 2022.

1. INTRODUCTION

As lithium-ion batteries mature into larger scale and variety of applications, the number and frequency of safety events have been increasing. [1] Our understanding of the sequence of events that contribute to battery failure and effective mitigation strategies is complicated by the multitude of failure events that occur in parallel, as well as the difficulty in reproducing these failure modes

accurately in laboratory tests. Over the years, mathematical models have been increasingly employed [2,3,4,5] to simulate the complex interplay of events such as response of vehicle batteries following a crash event or consumer electronic cells subject to mechanical shocks. In this study, we focus on the thermal response of cylindrical format cells under ultra-high strain-rate deformation.

There are several challenges unique to this system that differentiate its response from traditional lab-scale tests under quasi-static loading. First off, the mechanical properties

of the cell components (as well as the packaging material) are significantly different when measured under dynamic loading conditions. Secondly, the duration of electrical contact between the impactor and the battery is of the same order of magnitude as that for the mechanical events. This results in a different set of electrical pathways for shorting. The influence of strain-rates on the electrical and thermal events that follow, is well documented [6] even under quasi-static nail-penetration tests: slower nail speeds tend to result in longer durations across which the short-circuit evolves. There are additional factors such as the conductivity of the nail and the likelihood of the indenter acting as a thermal sink that complicate the outcome of these tests. These effects are only amplified under very high strain rates. Finally, because of the high shear-rates, the damage patterns across electrode layers are also different under extreme dynamic loading. This results in higher thermal impedance for these shorts.

In a previous report, we discussed the dynamic mechanical behavior of lithium-ion pouch cells subjected to high-velocity impact. [7] These results emphasized the importance of packaging and how anchoring of the electrodes within the cell in different commercial cell formats influenced their mechanical response. We also discussed the differences between the response of individual cells versus cells in a module. Given that the pouch-format cells offer inherently weaker mechanical resistance to deformation compared to those with a metal casing, these prior results motivated a follow-on study that focuses on cells with hard casing.

In this study, we report some results from mechanical deformation of cylindrical cells subject to deformation from impact under projectile loading with strain rates upwards of 100/s. We implement a scalable approach that allows for extension of the approach

presented here to realistic battery modules. We also discuss pressure and temperature build-up. We compute flame lengths as a function of gas compositions that change with the state-of-charge of the cells. We conclude with a comparison on how the abuse response changes with the type of failure even across different cells within the same module.

2. MODELING APPROACH

We use a 3P2S configuration of 18650 format cells as an example (Fig. 1) to demonstrate that the detailed modeling approach presented here can be scaled to study propagation across multiple cells.

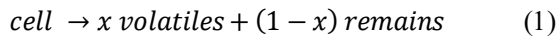


Figure 1: Geometry of the 3P2S configuration of 18650 cells used in this study and direction of loading under ultra-high strain-rates

We employ the explicit finite element code LS-DYNA to symmetrically study the deformation of the module under ultra-high strain-rates induced by projectile loading. A detailed discussion of the material properties for the electrodes, alongside a complete list of model equations to emulate the mechanical response was provided in earlier

publications. [7] The cell casing was aluminum with 100 μm thickness. We used shell elements for the cell-casing with a power-law representation of plasticity. The mechanical model consisted of about 18000 shell-elements after mesh-refinement, while the impactor was meshed with 54,228 tetrahedral solid elements. The computational nodes at the bottom surface were constrained with zero displacement and velocity conditions. The initial translational velocity for the projectile was set to 300 m/s along the x-direction. Under the high-velocity impact, the interactions between the impactor and the cell-casing as well as those between cells were defined by using the `ERODING_SURFACE_TO_SURFACE` card in LS-DYNA. The threshold for plastic failure strain was set to 0.4876 for element deletion.

The deformed geometry was imported into ANSYS/Fluent to perform the subsequent thermal runaway reactions. An RNG $k-\epsilon$ turbulence model [9] was used in the free-stream region and a Darcy-Forchheimer implementation [10-11] for the porous region. A complete set of model equations for the CFD simulations is provided in [8]. The electrode scale reactions are modeled as lumped heat source terms in a generic energy balance equation. Two different electrode scale models are considered in this study: i) gas pressure models inside the cell casing and ii) thermal abuse and gas generation models. we use a lumped one-step kinetic rate equation to represent thermal abuse and gas generation. The cell undergoes a single-step decomposition reaction notated as:



where volatiles are gases that are generated during thermal abuse reactions. The value x , the mass fraction of cell that turn into gas volatiles, is obtained by measuring the mass of generated gas from 18650 cell.

We modified the rate of abuse and heat generation developed by Hatchard et al. [12] for the one-step global expressions:

$$\frac{d\alpha}{dt} = -A_{ab}(\alpha)^m(1 - \alpha)^n \exp\left(-\frac{E_{a,ab}}{RT}\right) \exp(-B_{ab} \alpha) \quad (2)$$

$$\dot{S}_{heat,ab} = H_{ab} \frac{d\alpha}{dt} \quad (3)$$

where α is the degree of reaction progress, and H_{ab} is a specific heat release due to the thermal abuse reaction. Note that these are empirical lumped-form representations of heat generation calibrated to experimental datasets. [13]

Assuming that the rate of gas generation is proportional to the rate of the thermal abuse reaction, the volumetric rate of gas generation due to devolatilization is calculated as follows:

$$\dot{S}_{m,ab} = xW \frac{d\alpha}{dt} \quad (4)$$

where W is the initial density of the cell content. If the volatiles react quickly, the source term for each gaseous species can be expressed as:

$$\dot{S}_{g,i,ab} = Y_{i,eq} \dot{S}_{m,ab} \quad (5)$$

where $Y_{i,eq}$ is a mass fraction of a species- i at its equilibrium composition. We used the composition identified by Golubkov et al. [14] consisting of 6 different gas species (H_2 , CO_2 , CO , CH_4 , C_2H_4 , and C_2H_6).

We used a second-order upwind scheme to discretize all state variables except turbulent kinetic energy, turbulent dissipation rate and pressure. A second-order central differencing scheme is used for computing pressures at the faces of cell elements. For turbulent kinetic energy and turbulent dissipation rate, a first-order upwind scheme was employed. A bounded second-order implicit scheme was used for time stepping. The PISO algorithm

[15] is used for the pressure-velocity coupling.

3. RESULTS AND DISCUSSION

Accurate representation of the cell components without compromising scalability of the models is an on-going challenge for mechanical simulations. Detailed representation of each layer of the jellyroll invariably results in poor quality computational elements in the mesh – especially under dynamic loading conditions. A lumped representation of the jellyroll is often used as a first approximation [16]; however, it is difficult to specify failure thresholds for individual components using this approach. We reported [4] a representative-sandwich (RS) based approach in some of our earlier studies to circumvent this issue. Subsequent efforts point to the need for multiple such RS units to adequately capture the deformation modes.

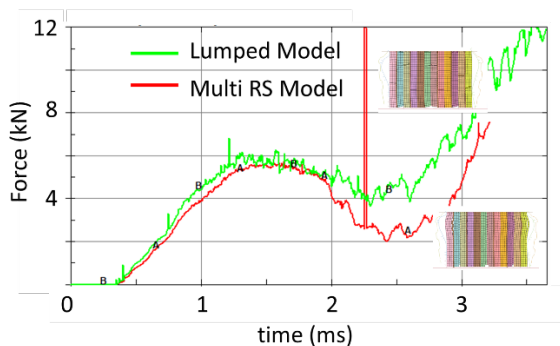


Figure 2: Comparison of the estimates for the resultant force versus time under dynamic impact loading, when the jellyroll is represented using A) a multiple RS model versus B) a lumped model

Some electrode-level simulation results are shown in Figure 2: there is not a significant difference in the resultant force between the multi-RS and the lumped models. However, the former captures details such as shear-induced failure and/or buckling in the in-plane direction better than the lumped formulation. For cylindrical cells, these failure modes are insignificant, compared to

other failure modes in the through-plane direction under ultra-high strain rates. Either of these approaches allow for a scalable implementation of the mechanical models at the module or pack scale, compared to the individual, layer-by-layer representation of the jellyroll.

Next, we move on to discuss the cell-level mechanical response. Figure 3 shows the deformed geometry after 100 ms from the onset of an ultra-high strain-rate impact at 300 m/s along the x-direction.

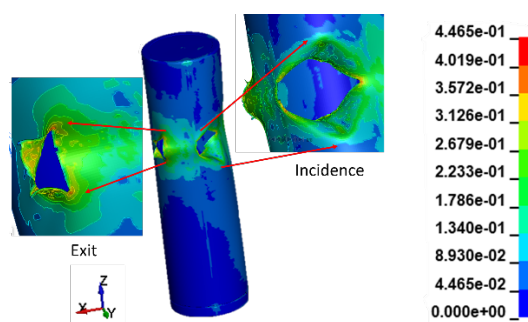


Figure 3: Maximum shear stress (MPa) mapped on to the deformed geometry of a single cell after 100 ms

In general, the simulation results capture the experimentally observed deformation patterns. An initial compressive failure in the through-plane direction normal to the surface of the can, is followed by in-plane tensile failure in the radial direction. Contours of the Tresca stresses show that the shear stresses at the interface between the impactor and the cell casing are high, as discussed in earlier sections. Of particular interest, is the fact that the projectile is able to pass through the cell and that the deformation of the cell can normal to the incident angle, results in secondary short-circuit pathways within the jellyroll.

Simulations at the multi-cell level show that cells not directly along the path of the projectile are subject to some shear and resultant deformation. For this set of simulations, these forces were sufficiently small not to result in any mechanical failure

of the cell wall in adjacent cells, reflecting the highly localized nature of the mechanical failure events. Cells 1,3 and 5, that were in the direct trajectory, did undergo mechanical failure, as anticipated.

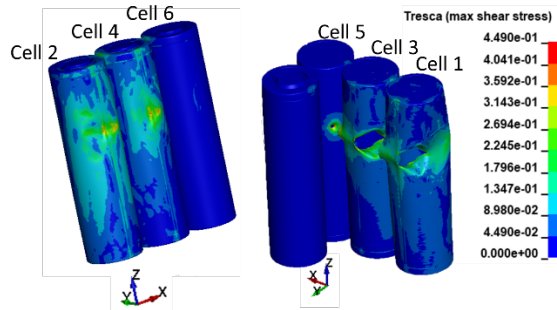


Figure 4: Multi-cell simulations showing the effect of shear stresses on adjacent cells not directly along the trajectory of the impactor

Comparison of the shear stresses for the single cell example on Figure 3, versus the multi-cell results on Figure 4 show that there is not a significant slowdown of the impactor. This was also reflected on the velocity of the indenter when plotted against time (not shown).

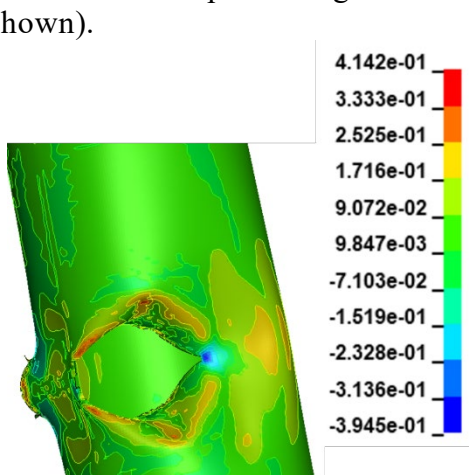


Figure 5: Gas pressure build-up near the point of incidence for a cell at 100% SOC: negative values indicate ejection of volatiles outside of the cell can

Build-up of gas pressure, for a single cell at 100% SOC is shown on Figure 5. As the volatiles are ejected out of the cell, there are localized areas showing negative pressure. The composition of the gas-phase ejecta is

determined by the maximum temperature within the cell (see equation 4).

Flammability limits (L_{gas}) can be calculated using the gas composition ($\dot{S}_{m,gas}$) knowing the standard limits for the individual components (L_i):[17]

$$L_{gas} = \frac{1}{\sum_{i=1}^n \frac{S_{mi}}{\rho_i L_i}} \quad (6)$$

For cells not directly subject to mechanical failure (Cells 2, 4 and 6) due to the impact, the venting events are controlled by the rate of temperature-rise due to venting of Cells 1, 3 and 5 as well as the maximum temperature from the mechanical impact. Indirect thermal failure resulting from propagation triggers secondary venting events, along the cell crimp once the internal pressure exceeds the design value for the seals. Thus, the cell-venting mechanism for Cells 1, 3 and 5 are controlled by mechanical impact; whereas that for Cells 2, 4 and 6 (in this case) are purely thermal.

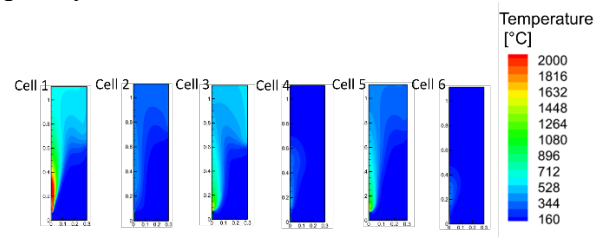


Figure 6: Gas phase temperature outside the individual cells 10 seconds after the onset of mechanical failure in Cell 1

4. CONCLUSIONS

In summary, we have reported a scalable framework to simulate the dynamic mechanical behavior of cylindrical lithium-ion cells subjected to ultra-high-velocity impact. These results have implications for design of battery modules in terms of determining mechanical fixturing for the individual cells, as well as design of vent thresholds or thickness of the casing for the cells. We did not consider other factors like

cell sizing, spacing between the cells, the effect of packaging, etc. in these simulations – but the methodology can readily be extended to these cases. Similarly, the results presented here are specific to the angle of incidence and velocity of the impactor; but the framework is sufficiently generic. Comparisons against experimental data is an on-going effort; but previous studies have extensively documented fragmenting of the cell casing and temperature rise comparable to results shown in here. The fire-safety models can be extended to compare mitigation strategies. At present, there are also limitations to the publicly available datasets. Nevertheless, this is the first attempt to predict outcomes at the module level for abuse response of batteries subject to mechanical deformation under ultra-high strain-rate.

5. ACKNOWLEDGEMENTS

This study was supported by the U.S. Army Ground Vehicle Systems Center (GVSC) project under contract number AC36-08GO28308. Some of the initial computational tools were originally developed under the Computer Aided Engineering for Batteries (CAEBAT) project of the Vehicle Technologies Office, Office of Energy Efficiency and Renewable Energy, U.S. Department of Energy under contract number WBS1.1.2.406. The research was performed using computational resources sponsored by the Department of Energy's Office of Energy Efficiency and Renewable Energy, located at the National Renewable Energy Laboratory.

The U.S. Government retains and the publisher, by accepting the article for publication, acknowledges that the U.S. Government retains a nonexclusive, paid up, irrevocable, worldwide license to publish or reproduce the published form of this work or allow others to do so, for U.S. Government purposes.

6. REFERENCES

- [1] EPRI, Program 94, “BESS Failure Event Database”, http://storagewiki.epri.com/index.php?title=BESS_Failure_Event_Database&oldid=1944. Retrieved March 2022.
- [2] T. Kisters, M. Gilaki, S. Nau, E. Sahraei, “Modeling of Dynamic Mechanical Response of Li-Ion cells with Homogenized Electrolyte-Solid Interactions”, *Journal of Energy Storage*, 104069, Vol. 49, 2022. <https://doi.org/10.1016/j.est.2022.104069>.
- [3] B. Liu, Y. Jia, C. Yuan, L. Wang, X. Gao, S. Yin, J. Xu, “Safety issues and mechanisms of lithium-ion battery cell upon mechanical abusive loading: A review” *Energy Storage Materials*, 24, 85-112, 2020.
- [4] H. Yin, S. Ma, H. Li, G. Wen, S. Santhanagopalan and C. Zhang, “Modeling strategy for progressive failure prediction in lithium-ion batteries under mechanical abuse.” *ETransportation*, 7, 100098.
- [5] D. Stephens, P. Shawcross, G. Stout, E. Sullivan, J. Saunders, S. Risser, and J. Sayre, “Lithium-ion battery safety issues for electric and plug-in hybrid vehicles”, Report No. DOT HS 812 418. Washington, DC: National Highway Traffic Safety Administration (NHTSA) 2017.
- [6] M. Rona, Y-F. Hyung, B. Barnett and S. Sriramulu, “The Relationship of the Nail Penetration Test to Safety of Li-Ion Cells”, Project id: ES142, Vehicle Technologies Office Annual Merit Review, 2013.
- [7] Y. Chen, S. Santhanagopalan, V. Babu, Y. Ding, “Dynamic mechanical behavior of lithium-ion pouch cells subjected to high-velocity impact”, *Composite Structures*, Vol. 218, 50-591, 2019. doi:10.1016/j.compstruct.2019.03.046.
- [8] J. Kim, A. Mallarapu, D.P. Finegan, S. Santhanagopalan, “Modeling cell venting and gas phase reactions in 18650 lithium ion batteries during thermal runaway”, *J. Power Sources*, Vol. 489, 229496, 2021.

- [9] V. Yakhot, S.A. Orszag, S. Thangam, T.B. Gatski, C.G. Speziale, “Development of turbulence models for shear flows by a double expansion technique”, *Phys. Fluids A*. Vol. 4, 1510–1520, 1992.
<https://doi.org/10.1063/1.858424>.
- [10] S. Whitaker, “The Forchheimer equation: A theoretical development”, *Transp. Porous Media*. Vol. 25, 27–61, 1996.
- [11] H. Darcy, “Les fontaines publiques de la ville de Dijon: Exposition et application des principes à suivre et des formules à employer dans les questions de distribution d’eau : Ouvrage terminé par un appendice relatif aux fournitures d’eau de plusieurs villes, au fil”, V. Dalmont, 1856.
<https://books.google.com/books?id=42EUA AAAQAAJ>
- [12] T.D. Hatchard, D.D. MacNeil, A. Basu, J.R. Dahn, “Thermal Model of Cylindrical and Prismatic Lithium-Ion Cells”, *J. Electrochem. Soc.* Vol. 148, A755-780, 2001. <https://doi.org/10.1149/1.1377592>.
- [13] G.H. Kim, A. Pesaran, R. Spotnitz, “A three-dimensional thermal abuse model for lithium-ion cells”, *J. Power Sources*. 170 476–489, 2007.
- [14] A.W. Golubkov, S. Scheikl, R. Planteu, G. Voitic, H. Wiltse, C. Stangl, G. Fauler, A. Thaler, V. Hacker, “Thermal runaway of commercial 18650 Li-ion batteries with LFP and NCA cathodes - Impact of state of charge and overcharge”, *RSC Adv*. Vol. 5, 57171–57186, 2015.
<https://doi.org/10.1039/c5ra05897j>
- [15] R.I. Issa, A.D. Gosman, A.P. Watkins, “The computation of compressible and incompressible recirculating flows by a non-iterative implicit scheme”, *J. Comput. Phys*. Vol. 62, 66–82, 1986.
- [16] T. Wierzbicki, E. Sahraei, “Homogenized mechanical properties for the jellyroll of cylindrical Lithium-ion cells”, *J. Power Sources*, Vol. 241, 467-476, 2013.
- [17] W. Li, H. Wang, Y. Zhang, M. Ouyang, “Flammability characteristics of the battery vent gas: A case of NCA and LFP lithium-ion batteries during external heating abuse”, *J. Energy Storage*, Vol. 24, 100775, 2019.